

Acoustically Induced Spin-Orbit Interactions Revealed by Two-Dimensional Imaging of Spin Transport in GaAs

H. Sanada,^{1,*} T. Sogawa,¹ H. Gotoh,¹ K. Onomitsu,¹ M. Kohda,² J. Nitta,² and P. V. Santos³

¹*NTT Basic Research Laboratories, NTT Corporation, 3-1 Morinosato-Wakamiya, Atsugi, Kanagawa 243-0198, Japan*

²*Department of Materials Science, Tohoku University, 6-6-02 Aramaki-Aza Aoba, Aoba-ku, Sendai 980-8579, Japan*

³*Paul-Drude-Institut für Festkörperelektronik, Hausvogteiplatz 5-7, 10117 Berlin, Germany*

(Received 22 November 2010; published 26 May 2011)

Magneto-optic Kerr microscopy was employed to investigate the spin-orbit interactions of electrons traveling in semiconductor quantum wells using surface acoustic waves (SAWs). Two-dimensional images of the spin flow induced by SAWs exhibit anisotropic spin precession behaviors caused by the coexistence of different types of spin-orbit interactions. The dependence of spin-orbit effective magnetic fields on SAW intensity indicates the existence of acoustically controllable spin-orbit interactions resulting from the strain and Rashba contributions induced by the SAWs.

DOI: 10.1103/PhysRevLett.106.216602

PACS numbers: 72.25.Dc, 71.70.Ej, 71.70.Fk, 77.65.Dg

The control of the spin-orbit interaction (SOI) in semiconductors is one of the keys to developing spintronics technologies [1] because it will greatly enhance spin lifetimes [2] and enable spin manipulation in ways that have been proposed for spin field-effect transistors [3], spin filters [4], and quantum computers [5]. The measurement of spin precession during carrier transport is a straightforward way of investigating SOIs in semiconductors. Conventional techniques involving spin transport under a dc-electric field [6] have been used to observe the spin precessions induced by SOI in the absence of an applied magnetic field [7]. Surface acoustic waves (SAWs) applied to semiconductor quantum wells (QWs) provide another way to transport electron spin coherence [8–10]. This method has the advantage of effectively suppressing the dominant spin relaxation process caused by the electron-hole exchange interaction [11], owing to the spatial separation of electrons and holes in the type-II-like lateral potential modulation created by the SAWs [8]. As a result, it has become possible to transport electrons acoustically over distances close to 100 μm while maintaining their spin coherence during precession around the effective magnetic fields caused by SOIs [9].

The effective magnetic field induced by any type of SOI can be used to manipulate the spin states of moving electrons. In systems with the Rashba SOI [12], the strength of the SOI can be controlled by an external gate voltage [13]. Recently, alternative SOIs induced by strain have been experimentally investigated in lattice mismatched heterostructures [7,14,15] and mechanically strained samples [16–18]. In contrast to the static strain fields used in these studies, SAWs provide dynamic strain and piezoelectric fields, thus opening the way for tuning the SOI by electrically adjusting the SAW intensity.

Measurements of the momentum direction dependence of SOIs have been widely used to determine their origins [7,14,15,19]. However, in the previous acoustic spin

transport experiments based on photoluminescence polarization measurements [8–10], a detailed analysis of the momentum direction dependence of the SOIs has been difficult to achieve, because the photoluminescence method requires special procedures for enhancing radiative recombination by locally screening the SAW-induced piezoelectric field. Here, we adopted the magneto-optic Kerr rotation (KR) method to explore the two-dimensional (2D) dynamics of traveling spins under SAWs over a wide range of acoustic amplitudes. This KR detection method does not require carrier recombination and so provides flexibility when we perform spatially resolved measurements of spins traveling in the QW plane. The present experiment, in which we precisely determined the SOIs with strengths of the order of 10^{-14} eV m, reveals the existence of spatially anisotropic SOIs as well as their dependence on SAW strength. A theoretical analysis of the experimental results elucidates the mechanisms of the acoustically controllable spin dynamics by taking into account the SAW-dependent SOIs induced by both the strain and Rashba contributions as well as the SAW-independent static SOIs.

The sample we studied was a 20-nm-thick undoped GaAs single QW with short-period GaAs/AlAs (30% average Al content) barriers grown by molecular-beam epitaxy on a (001) semi-insulating GaAs substrate. The QW was located 485 nm below the surface. A 50-nm-thick Al film deposited on top of the sample was processed by electron-beam lithography into interdigital transducers, which were designed for operation at a SAW wavelength of 2.55 μm and a frequency of 1.154 GHz. Rayleigh SAWs propagating along $[\pm 110]$ with a SAW velocity $|\mathbf{v}_{\text{SAW}}| = 2.9$ km/s produce “moving wires,” which are formed by 1D lateral confinement of the SAW-induced piezoelectric potential. The interference of two orthogonal SAW beams forms “moving dots” traveling along [010] with a velocity of $\sqrt{2}|\mathbf{v}_{\text{SAW}}|$ (Fig. 1, inset) [9].

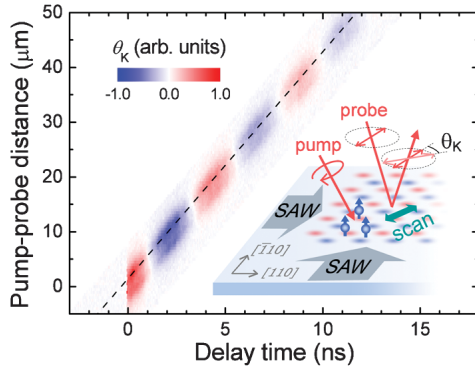


FIG. 1 (color). Spatiotemporal evolution of the KR signal for the moving dots traveling along [010]. The dashed line shows the slope determined by $\sqrt{2}|\mathbf{v}_{\text{SAW}}|$. Inset: The setup for spatially resolved KR measurements.

The spin dynamics during transport was measured by time- and spatially resolved KR microscopy using a mode-locked Ti:sapphire laser (1.5 ps, 82 MHz, 1.527 eV) as illustrated in the inset in Fig. 1. Circularly polarized pump pulses (an averaged power of 1.1 μW) were focused at a fixed position on the sample, while the KR angle of reflected linearly polarized probe pulses (0.9 μW) with a time delay was measured by using a balanced detection technique. The polarization of the pump light was modulated between left- and right-circular polarizations at 50.1 kHz, and the probe light was chopped by using an acousto-optic modulator at 52.0 kHz. The difference frequency (1.9 kHz) was used as a reference for lock-in detection. The full width at half maximum spot size of the normally incident probe beam was approximately 3 μm , whereas the waist size of the obliquely incident pump beam was 6 μm and its spot on the sample was slightly elongated along the [100] direction. The position of the probe light spot was scanned in the QW plane for spatially resolved KR measurements. For the 2D mapping of steady-state spin distributions, we adopted a two-color pump-probe method using a pair of cw Ti:sapphire lasers. All the measurements were carried out at 30 K in the absence of applied magnetic fields.

Figure 1 shows the spatiotemporal evolution of photo-injected spins trapped in the moving dots traveling along [010]. The slope of the KR signal in Fig. 1 indicates that the spin-polarized electrons move with the expected velocity of $\sqrt{2}|\mathbf{v}_{\text{SAW}}| = 4.14$ km/s. The oscillations with a period of about 4.5 ns are attributed to spin precession around the SO effective magnetic field. The data thus clearly demonstrate that our method successfully extracts information about the spin dynamics including spin transport and spin precession induced by SOIs.

Figure 2 compares the spatial mapping of the steady-state spin densities for moving wires [Figs. 2(a) and 2(c)] and moving dots [Fig. 2(b)]. In the two-color measurement, the pump energy was fixed at 1.527 eV, whereas the probe energy was tuned at 1.525, 1.526, and 1.528 eV for

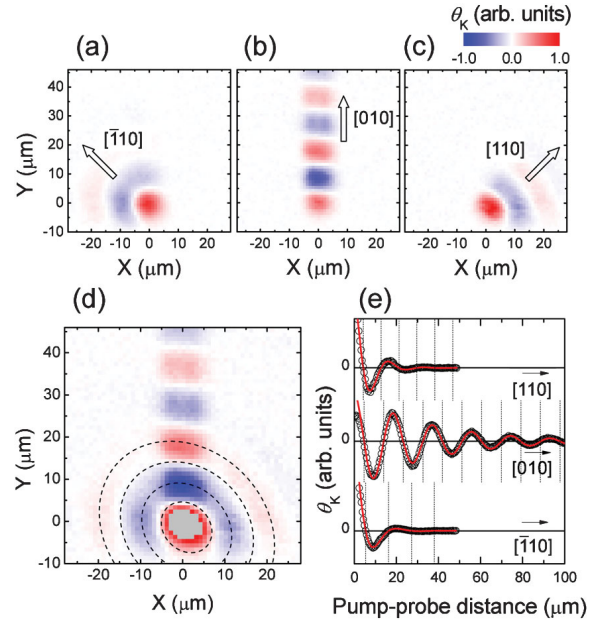


FIG. 2 (color). (a)–(d) 2D images of spin densities for moving wires traveling along $[\bar{1}10]$ (a), $[110]$ (c), and for moving dots traveling along $[010]$ (b). The sum of the data (a)–(c) is plotted in (d), where the dashed ellipses are guides to the eye. (e) Line cuts along the three directions in the data (a)–(c) are plotted (symbols) with fitted curves (red lines). The dashed lines represent precession phases of $\pi/2, (3/2)\pi, (5/2)\pi, \dots$

$[\bar{1}10]$, $[010]$, and $[110]$, respectively, because the band gap energies at the electron-trapping positions are modulated by SAW fields [20]. The pump (probe) power was 20 (0.9) μW , respectively. In contrast to the well-confined carrier transport by moving dots [Fig. 2(b)], carriers in moving wires diffuse rapidly along the wire axis [Figs. 2(a) and 2(c)]. Though the KR signal for the wires is reduced by the carrier diffusion, we can access the momentum direction dependences of spin precessions [Fig. 2(d)], where the sum of the mapping data [Figs. 2(a)–2(c)] shows that the isophase lines have clear elliptical shapes. In Fig. 2(e), the KR angles θ_K (open circles) along the particular axes ($[\bar{1}10]$, $[010]$, and $[110]$) are fitted with a function $\theta_K(d) = \theta_0 \cos(2\pi\kappa d) \times \exp(-d/L_s)$, where d is the pump-probe distance and L_s and κ are fitting parameters representing the spin decay length and spatial precession frequency, respectively. We obtained $\kappa_{[\bar{1}10]} = 0.0589 \pm 0.0008$, $\kappa_{[010]} = 0.05369 \pm 0.00009$, and $\kappa_{[110]} = 0.0460 \pm 0.0006 \mu\text{m}^{-1}$, for the traveling directions $[\bar{1}10]$, $[010]$, and $[110]$, respectively. Since κ is proportional to the SO effective magnetic field, these results demonstrate that the SOIs are spatially anisotropic in the present system.

The SOI dependence on the traveling direction is known to be caused by the coexistence of different types of SOIs [7,14,15,19]. For electrons confined in (001) QWs, the momentum-dependent effective magnetic field $\mathbf{\Omega}_{\text{so}}(\mathbf{k})$ is primarily determined by k -linear terms, which are classified into two types [21]:

$$\mathbf{\Omega}^\alpha(\mathbf{k}) = \frac{2\alpha}{\hbar} \begin{pmatrix} k_Y \\ -k_X \\ 0 \end{pmatrix}, \quad \mathbf{\Omega}^\beta(\mathbf{k}) = \frac{2\beta}{\hbar} \begin{pmatrix} -k_X \\ k_Y \\ 0 \end{pmatrix}, \quad (1)$$

where we used a coordinate system with base vectors $\hat{X} \parallel [100]$, $\hat{Y} \parallel [010]$, and $\hat{Z} \parallel [001]$. Figure 3 shows the orientation dependence of $\mathbf{\Omega}^\alpha(\mathbf{k})$ and $\mathbf{\Omega}^\beta(\mathbf{k})$ in \mathbf{k} space. Since these vectors have different dependences on the direction of \mathbf{k} , their coexistence leads to the twofold symmetry of $|\mathbf{\Omega}^\alpha(\mathbf{k}) + \mathbf{\Omega}^\beta(\mathbf{k})|$ as illustrated in Fig. 3. In general, $\mathbf{\Omega}^\alpha(\mathbf{k})$ and $\mathbf{\Omega}^\beta(\mathbf{k})$ are mainly induced by the structural inversion asymmetry caused by a static electric field [Rashba SOI [12], as described by Eq. (1) with an SOI parameter α_R] and the intrinsic bulk inversion asymmetry (Dresselhaus SOI [22] described by β_D), respectively. In the present system, we consider three additional contributions described by α_R^{SAW} , α_S^{SAW} , and β_S^{SAW} : α_R^{SAW} is induced by the vertical component of the SAW piezoelectric field F_Z^{piezo} , and α_S^{SAW} (β_S^{SAW}) is induced by the off-diagonal (diagonal) components of strain tensor $\tilde{\epsilon}$ [23–25]. Hence, α and β in Eq. (1) are given by the sum of the contributions, i.e., $\alpha = \sum \alpha_i$ and $\beta = \sum \beta_i$.

As expected, κ varies with the SAW intensities P_{SAW} , which is defined as the acoustic power flux per unit length along the cross section of the SAW beam. The symbols in Fig. 4(a) represent experimentally obtained $\kappa_{[010]}$, $\kappa_{[110]}$, and $\kappa_{[\bar{1}10]}$ versus $\sqrt{P_{\text{SAW}}}$, which is proportional to the amplitude of the SAW piezoelectric and strain fields. We estimated P_{SAW} from the band gap shift observed in photoluminescence spectra [26]. As P_{SAW} increases, $\kappa_{[010]}$ ($\kappa_{[\pm 110]}$) monotonically increases (decreases), suggesting that the SOI is acoustically controllable. We also found that $\kappa_{[110]}$ and $\kappa_{[\bar{1}10]}$ do not coincide even if we reduce P_{SAW} , thus indicating the presence of a second SAW-independent contribution in addition to β_D . We will assume this contribution to be of the α type (described by α_0). It may be composed of the static Rashba term α_R induced by the carrier-induced band bending and another SOI term that has its origin in the unintentional static strain introduced during the sample mounting and/or cooling processes.

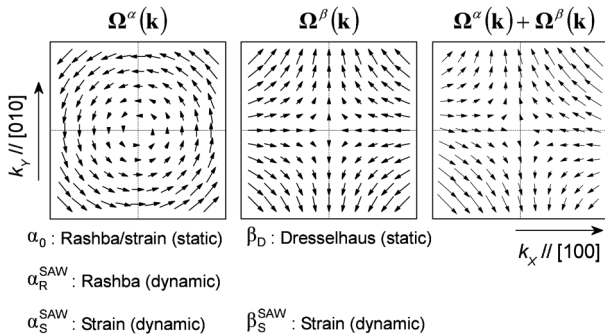


FIG. 3. Effective magnetic fields $\mathbf{\Omega}^\alpha$, $\mathbf{\Omega}^\beta$, and $\mathbf{\Omega}^\alpha + \mathbf{\Omega}^\beta$ are plotted as vectors in \mathbf{k} space. $\alpha < 0$, $\beta > 0$, and $\beta > |\alpha|$ are assumed in this figure.

To extract the acoustically induced SOIs from the experimental results, we estimated each SOI contribution to the spin precessions as follows. From the calculation of the Rayleigh SAW fields including the piezoelectric coupling [27], we obtain the components of $\tilde{\epsilon}$ and the vertical piezoelectric field F_Z^{piezo} at the potential energy minima of the moving dots and wires. The calculated $\tilde{\epsilon}(P_{\text{SAW}})$ and $F_Z^{\text{piezo}}(P_{\text{SAW}})$ yield $\alpha_R^{\text{SAW}}(P_{\text{SAW}})$, $\alpha_S^{\text{SAW}}(P_{\text{SAW}})$, and $\beta_S^{\text{SAW}}(P_{\text{SAW}})$ [28] in accordance with the relations $\alpha_R^{\text{SAW}} = -r_{41}^{6c6c}[(\Delta E_c + \Delta E_v)/\Delta E_c]F_Z^{\text{piezo}}$ (ΔE_c and ΔE_v represent conduction and valence band offsets, respectively) [21], $\alpha_S^{\text{SAW}} = C_3 \epsilon_{XY}/2$, and $\beta_S^{\text{SAW}} = D(\epsilon_{XX} - \epsilon_{ZZ})$ [23–25]. Here, the following material constants were used: $r_{41}^{6c6c} = 5.206 \times 10^{-20} e \text{ m}^2$ [21], $(\Delta E_c + \Delta E_v)/\Delta E_c = 1.636$, $C_3 = 8.1 \times 10^{-10} \text{ eV m}$ [17], and $D = 6.6 \times 10^{-12} \text{ eV m}$ [25]. We also estimated the P_{SAW} dependence of $\beta_D = \gamma \langle k_Z^2 \rangle$, where γ is the material constant and $\langle k_Z^2 \rangle$ is the expectation value of the operator $k_Z^2 = -(\partial^2/\partial Z^2)$. The SAW-induced F_Z^{piezo} modifies the electron wave function along the Z axis. However, the calculated changes in β_D are negligible compared with those in α_R^{SAW} and α_S^{SAW} . To fit the previous expressions to the data in Fig. 4(a), we used the two P_{SAW} -independent parameters as fitting parameters: The first is $\beta_D = 1.85 \times 10^{-13} \text{ eV m}$, from which we extract $\gamma = 1.16 \times 10^{-29} \text{ eV m}^3$ [29,30]. The other parameter $\alpha_0 = -2.5 \times 10^{-14} \text{ eV m}$ is the static component of α that was discussed above.

The calculated results [Fig. 4(b)] reveal the contributions of the SOI parameters (α_R^{SAW} , α_S^{SAW} , α_0 , β_D , and β_S^{SAW}) to the total SOI. Since ϵ_{XY} , ϵ_{XX} , ϵ_{YY} , ϵ_{ZZ} , and F_Z^{piezo} are proportional to $\sqrt{P_{\text{SAW}}}$, the calculated α_R^{SAW} , α_S^{SAW} , and β_S^{SAW} show a linear dependence on $\sqrt{P_{\text{SAW}}}$. The notable increases in $|\alpha_R^{\text{SAW}}|$ and $|\alpha_S^{\text{SAW}}|$ with increasing

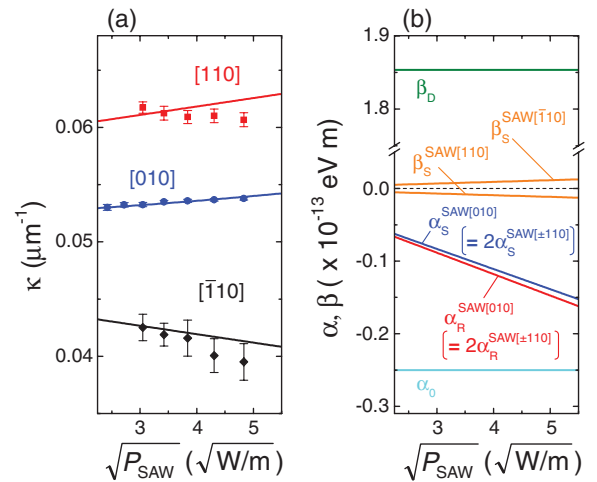


FIG. 4 (color). (a) The data for P_{SAW} dependence of $\kappa_{[010]}$, $\kappa_{[110]}$, and $\kappa_{[\bar{1}10]}$ are plotted with calculated lines. The error bars for the data represent two standard errors of the parameters obtained from a least-squares fitting. (b) P_{SAW} dependence of the SO parameters obtained by the calculations.

P_{SAW} indicate that α_R^{SAW} and α_S^{SAW} should be the dominant sources of SAW-induced SOI. Compared with the parameters (F_Z^{piezo} , ε_{XY} , ε_{XX} , and ε_{ZZ}) produced by a single SAW beam, the superposition of the two SAW beams doubles F_Z^{piezo} and ε_{XY} , whereas it cancels ε_{XX} and ε_{ZZ} at the potential minimum of the moving dots. Thus, we obtain the relations $\alpha_{R(S)}^{\text{SAW}[010]} = 2\alpha_{R(S)}^{\text{SAW}[\pm 110]}$, $\beta_S^{\text{SAW}[110]} = -\beta_S^{\text{SAW}[\bar{1}\bar{1}0]}$, and $\beta_S^{\text{SAW}[010]} = 0$.

The solid lines in Fig. 4(a) represent the κ values calculated by using the SOI parameters of Fig. 4(b). Note that the changes in κ calculated for the moving dots well reproduce the experimental data. The corresponding changes in α_R^{SAW} or α_S^{SAW} under the present experimental conditions are only approximately 10^{-14} eV m. Our experimental method is, therefore, highly sensitive to the changes in the SOIs. We also found that the slope of $\kappa(P_{\text{SAW}})$ for the moving dots is not as steep as those for the moving wires. This occurs because Ω^α fields related to $\alpha_R^{\text{SAW}[010]}$ and $\alpha_S^{\text{SAW}[010]}$ are orthogonal to the strong Ω^β determined by the Dresselhaus contribution β_D . For the moving wires, in contrast, all contributions lie along the same direction perpendicular to the SAW propagation. However, the carrier diffusion along the wires prevents the long-distance spin transport.

In contrast to the good agreement obtained for the moving dots, there are certain discrepancies between the experimental data and the calculations for the moving wires, which are not yet fully understood. We should consider that the rapid decrease in the carrier density due to the lateral diffusion in the moving wires, as observed in Figs. 2(a) and 2(c), might influence the spin dynamics through the modulation of the Rashba contribution with the carrier-density-dependent band bending. Another possible origin is the SAW-induced strain gradient along \hat{Z} [7]. The strain gradient leads to structural inversion asymmetry and thus introduces another SAW controllable SOI. Consequently, there should be additional contributions similar to Ω^α and Ω^β , which are proportional to $\partial\varepsilon_{XY}/\partial Z$ and $\partial\varepsilon_{ii}/\partial Z$, respectively. Further studies and theoretical developments are needed to explore the relevant mechanisms.

In conclusion, we have studied the SOIs of electrons traveling in semiconductor QWs using SAW fields. The time- and/or spatially resolved KR technique enabled the 2D imaging of the traveling spins, which revealed anisotropic spin precession behavior resulting from the coexistence of different types of SOIs. The dependence of the precession frequencies on SAW intensity was analyzed based on a theoretical model, indicating that the strength of the SOIs due to strain and Rashba contributions can be tuned by adjusting the SAW intensity. The demonstrated experimental method is beneficial for further investigation of acoustically induced SOIs in semiconductors. It will also provide the flexibility needed for spin manipulation via dynamically controlled SOIs in future spintronics applications.

We thank Y. Tokura, H. Yamaguchi, and T. Tawara for useful discussions. This work received support from the Japan Society for the Promotion of Science (JSPS).

*sanada.haruki@lab.ntt.co.jp

- [1] S. A. Wolf *et al.*, *Science* **294**, 1488 (2001).
- [2] J. D. Koralek *et al.*, *Nature (London)* **458**, 610 (2009); Y. Kunihashi, M. Kohda, and J. Nitta, *Phys. Rev. Lett.* **102**, 226601 (2009).
- [3] S. Datta and B. Das, *Appl. Phys. Lett.* **56**, 665 (1990).
- [4] T. Koga *et al.*, *Phys. Rev. Lett.* **88**, 126601 (2002); J. Ohe *et al.*, *Phys. Rev. B* **72**, 041308 (2005).
- [5] D. Stepanenko and N. E. Bonesteel, *Phys. Rev. Lett.* **93**, 140501 (2004).
- [6] J. M. Kikkawa and D. D. Awschalom, *Nature (London)* **397**, 139 (1999); D. Hägele *et al.*, *Appl. Phys. Lett.* **73**, 1580 (1998); H. Sanada *et al.*, *ibid.* **81**, 2788 (2002).
- [7] Y. Kato *et al.*, *Nature (London)* **427**, 50 (2004).
- [8] T. Sogawa *et al.*, *Phys. Rev. Lett.* **87**, 276601 (2001).
- [9] J. A. H. Stotz *et al.*, *Nature Mater.* **4**, 585 (2005).
- [10] O. D. D. Couto, Jr. *et al.*, *Phys. Rev. Lett.* **98**, 036603 (2007).
- [11] G. L. Bir, A. G. Aronov, and G. E. Pikus, *Zh. Eksp. Teor. Fiz.* **69**, 1382 (1975) [*Sov. Phys. JETP* **42**, 705 (1975)].
- [12] Y. A. Bychkov and E. I. Rashba, *J. Phys. C* **17**, 6039 (1984).
- [13] J. Nitta *et al.*, *Phys. Rev. Lett.* **78**, 1335 (1997).
- [14] L. Meier *et al.*, *Nature Phys.* **3**, 650 (2007).
- [15] B. M. Norman *et al.*, *Phys. Rev. B* **82**, 081304(R) (2010).
- [16] S. A. Crooker and D. L. Smith, *Phys. Rev. Lett.* **94**, 236601 (2005).
- [17] M. Beck *et al.*, *Europhys. Lett.* **75**, 597 (2006).
- [18] V. Sih *et al.*, *Phys. Rev. B* **73**, 241316(R) (2006).
- [19] S. D. Ganichev *et al.*, *Phys. Rev. Lett.* **92**, 256601 (2004); M. Scheid *et al.*, *ibid.* **101**, 266401 (2008); M. Studer *et al.*, *ibid.* **103**, 027201 (2009).
- [20] F. Alsina, P. V. Santos, and R. Hey, *Phys. Rev. B* **65**, 193301 (2002).
- [21] R. Winkler, *Spin-Orbit Coupling Effects in 2D Electron and Hole Systems* (Springer, Berlin, 2003).
- [22] G. Dresselhaus, *Phys. Rev.* **100**, 580 (1955).
- [23] G. E. Pikus and A. N. Titkov, in *Optical Orientation*, edited by F. Meier and B. P. Zakharchenya (Elsevier, Amsterdam, 1984).
- [24] G. C. La Rocca, N. Kim, and S. Rodriguez, *Phys. Rev. B* **38**, 7595 (1988).
- [25] B. A. Bernevig and S.-C. Zhang, *Phys. Rev. B* **72**, 115204 (2005).
- [26] T. Sogawa *et al.*, *Phys. Rev. B* **63**, 121307(R) (2001).
- [27] S. H. Simon, *Phys. Rev. B* **54**, 13878 (1996).
- [28] O. D. D. Couto, Jr., R. Hey, and P. V. Santos, *Phys. Rev. B* **78**, 153305 (2008).
- [29] Though we consider only the \mathbf{k} -linear Dresselhaus term here, the β value may be reduced by the \mathbf{k} -cubic term as reported in the work by M. Studer *et al.* [30], which was published after the submission of this Letter.
- [30] M. Studer *et al.*, *Phys. Rev. B* **82**, 235320 (2010).